A turbulence model taking into account the longitudinal flow inhomogeneity in mixing layers and jets

A. I. Troshin
Central Aerohydrodynamic Institute (TsAGI)
1 Zhukovsky Street, Zhukovsky, Moscow Region, 140180, Russia
ai-troshin@yandex.ru

Abstract

The problem of potential core length overestimation of subsonic free jets by RANS-based turbulence models is addressed. It is shown that the issue is due to the incorrect velocity profile modeling of the jet mixing layers. An additional source term in ω equation is proposed which takes into account the effect of longitudinal flow inhomogeneity on turbulence in mixing layers. Computations confirm that the modified SSG/LRR-ω turbulence model correctly predicts the mean velocity profiles in both the initial and far field regions of subsonic free plane jet as well as the centerline velocity decay rate.

1. Introduction

Many RANS-based turbulence models overestimate the potential core length of subsonic free jets.[1] Analysis shows that this issue is due to incorrect velocity profile modeling of the jet mixing layers.[2,3] To solve this problem, a correction which increases the turbulence diffusion intensity near the jet axis is proposed in Ref. 1, unfortunately not Galilean invariant. In Ref. 3, an invariant correction is suggested which enhances the turbulence diffusion at the edges of turbulent regions and recovers the velocity profile of a single stream mixing layer.

In this paper, a further investigation is conducted. Another way to reduce the jet potential core length in computations is proposed which is not connected to the modification of turbulence diffusion coefficients. Instead, an additional source term in characteristic turbulence frequency equation is proposed. The differential Reynolds stress model (DRSM) SSG/LRR-ω[4] is taken as the basis for improvement. This is a modern DRSM with a great potential in modeling complex problems with non-equilibrium turbulence, separation, secondary flows and streamline curvature. SSG/LRR-ω model uses a blending function to switch between the near-wall and free turbulent coefficient values. In the present study, only "free turbulent part" of the model is modified.

The structure of the paper is as follows. In Section 2, the equations of the original SSG/LRR-ω model are quoted as well as the results of self-similar computations of mixing layers and a plane jet. In Section 3, a calibration of model coefficients is conducted using the temporal mixing layer data. In Section 4, an additional source term in ω equation is developed which improves the spatial mixing layer velocity profile. Finally, in Section 5 the computations using the complete Reynolds equation system closed by the modified turbulence model are presented, and the improvements are shown which result from the changes made.

2. SSG/LRR-ω model performance in free turbulent flows

The original SSG/LRR-ω model equations are as follows[4]:

$$\frac{\partial \bar{\rho} R_{ij}}{\partial t} + \frac{\partial}{\partial x_k}\left(\bar{\rho} R_{ij}\bar{u}_k - \mu\frac{\partial R_{ij}}{\partial x_k} - C_R\bar{\rho}\frac{k}{\varepsilon}R_{kl}\frac{\partial R_{ij}}{\partial x_l}\right) = \bar{\rho}\left(P_{ij} + \Pi_{ij} - \frac{2}{3}\varepsilon\delta_{ij}\right), \tag{1}$$

$$\frac{\partial \bar{\rho}\omega}{\partial t} + \frac{\partial}{\partial x_k}\left(\bar{\rho}\omega\bar{u}_k - \mu\frac{\partial \omega}{\partial x_k} - C_\omega\bar{\rho}\frac{k^2}{\varepsilon}\frac{\partial \omega}{\partial x_k}\right) = \bar{\rho}\frac{\omega}{k}\left(C_{\omega 1}P - C_{\omega 2}\varepsilon\right) + \frac{\alpha_d C_\omega}{C_\mu}\frac{\bar{\rho}}{\omega}\max\left(\frac{\partial k}{\partial x_k}\frac{\partial \omega}{\partial x_k}, 0\right). \tag{2}$$

Hereinafter summation over repeated indices is adopted. $R_{ij} = \overline{u'_i u'_j}$ is Reynolds stress tensor, ω is characteristic turbulence frequency, $k = R_{ii}/2$ is turbulence kinetic energy and $\varepsilon = C_\mu k\omega$ is its dissipation rate ($C_\mu = 0.09$). Reynolds stress production is computed according to the exact formula

$$P_{ij} = -R_{ik}\frac{\partial \bar{u}_j}{\partial x_k} - R_{jk}\frac{\partial \bar{u}_i}{\partial x_k}. \tag{3}$$

Turbulence kinetic energy production is $P = P_{ii}/2$. Redistribution term Π_{ij} is computed using SSG model[5] in free turbulent regions and LRR model with coefficients proposed by D. C. Wilcox[6] in near-wall regions.

Coefficient values are presented in the Table 1.

Table 1: The original SSG/LRR-ω model coefficients

	$C_{\omega 1}$	$C_{\omega 2}$	C_R	C_ω	α_d
Near-wall turbulence	0.5556	0.8333	0.0675	0.045	0
Free turbulence	0.44	0.92	0.22	0.077	2.0

This turbulence model has been used to compute 3 free turbulent incompressible self-similar flows. The first is temporal mixing layer which forms between two parallel streams with almost equal velocities $|u_2 - u_1| \ll u_1 + u_2$.[7] In the coordinate frame moving with velocity $(u_1 + u_2)/2$ and y axis normal to the flows, the mixing layer is symmetrical relative to its center, longitudinal gradients of every flow variable and transverse velocity component are negligible, and mixing zone thickness linearly grows with time. To compute the self-similar temporal mixing layer velocity profile, it is sufficient to solve only the longitudinal momentum equation supplied by the shear stress profile:

$$\frac{\partial \bar{u}}{\partial t} + \frac{\partial R_{xy}}{\partial y} = 0. \tag{4}$$

Let us introduce the self-similar variables $\tau = t$, $\eta = y/(u_0 t)$, where $u_0 > 0$ is the velocity of either stream in the chosen coordinate frame, and denote $f(\eta) = \bar{u}(t,y)/u_0$, $r_{ij}(\eta) = R_{ij}(t,y)/u_0^2$. In these variables, Equation (4) takes form

$$-\eta f' + r'_{xy} = 0. \tag{5}$$

Equations (1) and (2) used to close this equation, are converted similarly.

Two other flows are the spatial single-stream mixing layer (Figure 1, a) and the far field region of a free plane jet (Figure 1, b). Both of them are inhomogeneous in longitudinal direction and contain non-zero transverse (ejection) velocity component v_e.

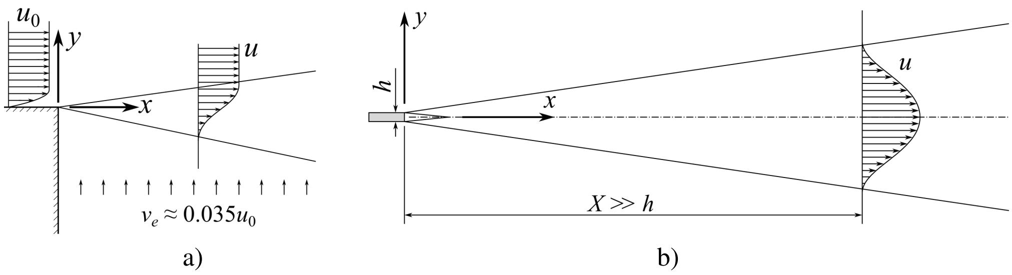

Figure 1: Flow field scheme of: a) single-stream mixing layer, b) free plane jet far field

The equation system describing these flows is the following:

$$\frac{\partial \bar{u}}{\partial x} + \frac{\partial \bar{v}}{\partial y} = 0, \tag{6}$$

$$\bar{u}\frac{\partial \bar{u}}{\partial x} + \bar{v}\frac{\partial \bar{u}}{\partial y} + \frac{1}{\bar{\rho}}\frac{\partial p}{\partial x} + \frac{\partial R_{xx}}{\partial x} + \frac{\partial R_{xy}}{\partial y} = 0, \tag{7}$$

$$\bar{u}\frac{\partial \bar{v}}{\partial x} + \bar{v}\frac{\partial \bar{v}}{\partial y} + \frac{1}{\bar{\rho}}\frac{\partial p}{\partial y} + \frac{\partial R_{xy}}{\partial x} + \frac{\partial R_{yy}}{\partial y} = 0. \tag{8}$$

Again, let us use the self-similar variables $\xi = x$, $\eta = y/x$ and denote $\bar{u}(x,y) = Ax^b f(\eta)$, $\bar{v}(x,y) = Ax^b g(\eta)$, $R_{ij}(x,y) = Bx^{2b} r_{ij}(\eta)$, $\omega(x,y) = Cx^{3b-1}w(\eta)$, $F = (f^2 + g^2)^{1/2}$, $\kappa = r_{ii}/2$. For the mixing layer, $b = 0$. For the plane jet, $b = -1/2$. We use the only simplification of (6)–(8):

$$\frac{1}{\bar{\rho}}\frac{\partial p}{\partial x} = -\frac{\partial R_{yy}}{\partial x}. \tag{9}$$

No other assumptions leading to "thin-shear-flow" approximation are used because they can distort the solution by as much as 12%.[8]

In (ξ, η)-variables, Equations (6)–(8) read

$$bf - \eta f' + g' = 0, \tag{10}$$

$$bf^2 + (g - \eta f)f' + 2b(r_{xx} - r_{yy}) - \eta(r'xx - r'yy) + r'_{xy} = 0. \tag{11}$$

Equations (1) and (2) are converted similarly.

A program has been implemented which solves Equations (5), (10) and (11) using time marching. An explicit second-order spatial scheme is adopted. At the external boundaries, very weak isotropic turbulence is specified: $r_{ij\infty} = 2\kappa_\infty\delta_{ij}/3$, $\kappa_\infty \ll \kappa_{\max}$, $w_\infty \ll w_{\max}$, where $\kappa_{\max}$ and $w_{\max}$ are the maximal values of κ and w in the whole computational domain. It is checked that the solutions obtained within turbulent zones are insensitive to the κ_∞ and w_∞ chosen as described.

A mesh convergence study has been performed, resulting in the decision to use the meshes containing 150 nodes within the turbulent zone.

In Figure 2, velocity profiles obtained with SSG/LRR-ω model are compared with the experimental data (Ref. 9 for temporal mixing layer, the same as in Ref. 3 for the other flows). The temporal mixing layer is plotted using the scaled coordinate $\eta^* = f'(0)\eta$ which makes the velocity slope in the center equal 1. From the data presented, the following conclusions can be made:

1. SSG/LRR-ω model predicts too sharp turbulent zone boundaries. This problem is evident in all the flows considered.

2. The low-velocity part of the spatial mixing layer is wider than the high-velocity part. Note that this shortcoming is inherent to virtually all differential turbulence models.[3,6]

3. Spatial mixing layer width is underestimated.

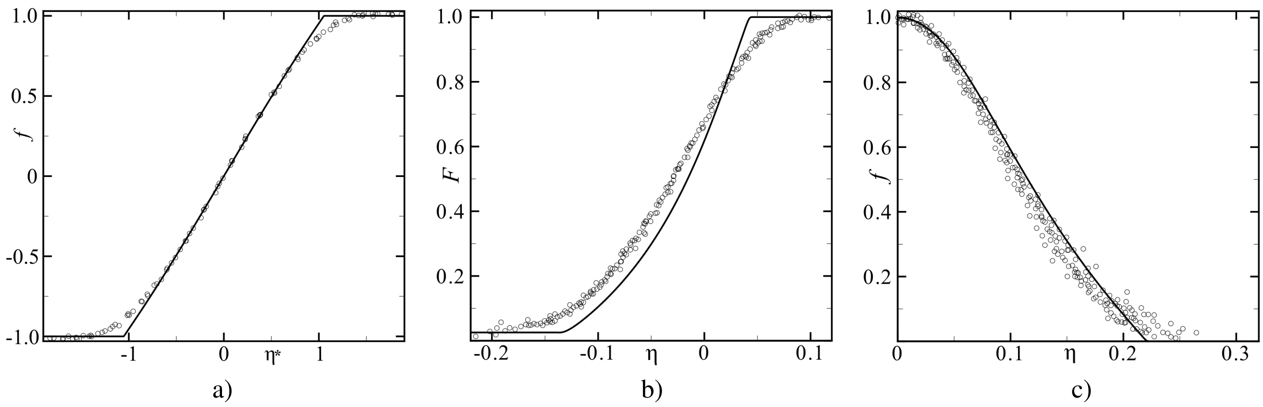

Figure 2: Self-similar solutions obtained with the original SSG/LRR-ω model: a) temporal mixing layer, b) single-stream mixing layer, c) free plane jet far field

Turbulent zone boundaries can be smoothed by calibrating the turbulent diffusion coefficients C_R, C_ω and α_d. In the following section, this is done using the simplest flow considered, namely temporal mixing layer.

3. Coefficients calibration using temporal mixing layer data

3 series of temporal mixing layer computations have been conducted, in which coefficients C_R, C_ω and α_d have been successively varied. The influence of these coefficients is shown in Figure 3.

C_R changes the velocity profile very strongly. Its influence appears not only near the turbulent zone boundaries, but spreads deeply inside it. As a result, it is impossible to obtain an accurate velocity profile which would fully conform to the experimental data by varying C_R only.

C_ω determines the velocity profile behavior only near the turbulent zone boundaries, and there is "saturation" at high C_ω values, when velocity profile becomes practically straight and does not change any further.

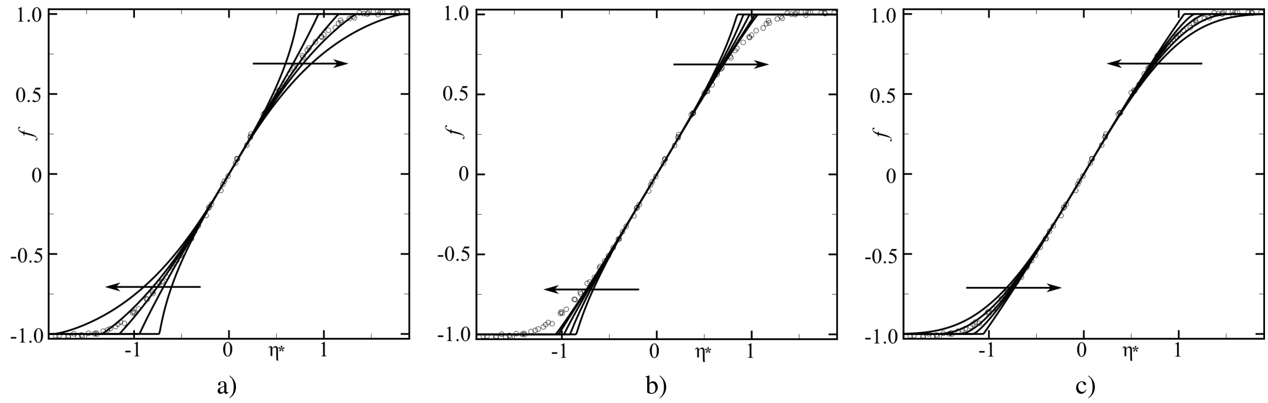

Figure 3: Influence of the coefficient: a) C_R, b) C_ω, c) α_d. Arrows indicate the direction of coefficient increase

α_d plays crucial role in velocity profile shaping. It influences its boundaries allowing to make it either sharp or very smooth.

To find the family of coefficient sets giving the temporal mixing layer velocity profile lying in the experimental data range, a series of parametric computations has been conducted.

In each computation, fixed values of C_R and C_ω have been set, and α_d adjusted so that $\eta^*_{0.99}$ coordinate (a boundary point where $f = 0.99$) would be equal, according to experiments, 1.36. As a result, for the values $C_R = 0.14$, 0.18, 0.20, 0.22 and 0.26 the curves $\alpha_d(C_\omega)$ have been obtained, points on which corresponding to temporal mixing layer velocity profiles with correct boundary positions. The diagram consisting of these curves is shown in Figure 4.

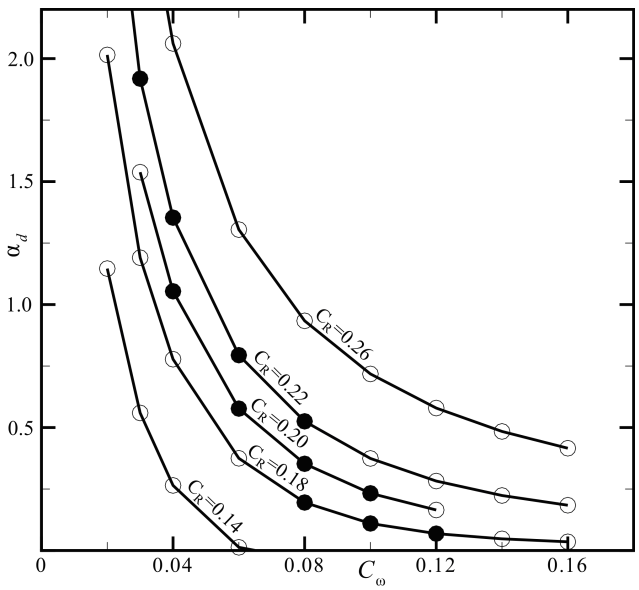

Figure 4: A diagram of SSG/LRR-ω model calibration using the temporal mixing layer data

Since the condition $\eta^*_{0.99} = 1.36$ does not fully determine the velocity profile, among the coefficient sets found, there are ones which give distorted velocity profiles in the regions between the center of the turbulent zone and its boundaries. The region of coefficient sets giving velocity profiles entirely matching the experimental data is marked on the diagram with black circles. The distribution of the black circles on the diagram indicates that in the $0.18 \leq C_R \leq 0.22$ range, accurate temporal mixing layer modeling is possible.

4. Taking into account the longitudinal flow inhomogeneity

The first step to calibrate the coefficients of the SSG/LRR-ω model using the spatial single-stream mixing layer data is to determine the α_d value provided $C_{\omega 1} = 0.48$ and $C_{\omega 2} = 0.86$ so that the mixing layer thickness $D_{0.1}$ computed by the points where $F = 0.1$ and 0.9 would be equal to the experimental value 0.165. The $C_{\omega 1}$ and $C_{\omega 2}$ values are taken from the middle of the “generally accepted” ranges $0.44 \leq C_{\omega 1} \leq 0.52$, $0.80 \leq C_{\omega 2} \leq 0.92$.[6] α_d appeared to be equal to

0.566. From the diagram (Figure 4), it follows that $C_R = 0.20$ and $C_\omega = 0.0593$. The velocity profile of single-stream mixing layer computed with these coefficient values is presented in Figure 5, a (the curve denoted as "without $I_\omega^{(0)}$"). It has the drawback which has already been noticed: the turbulent zone spreads too strongly towards the low-velocity region of the mixing layer and too weakly towards the high-velocity region. The potential core length estimation using this velocity profile is $L_{\text{ini}} = 8.46$ which is about 1.5 times higher than experimental values $5 \leq L_{\text{ini}} \leq 6$.

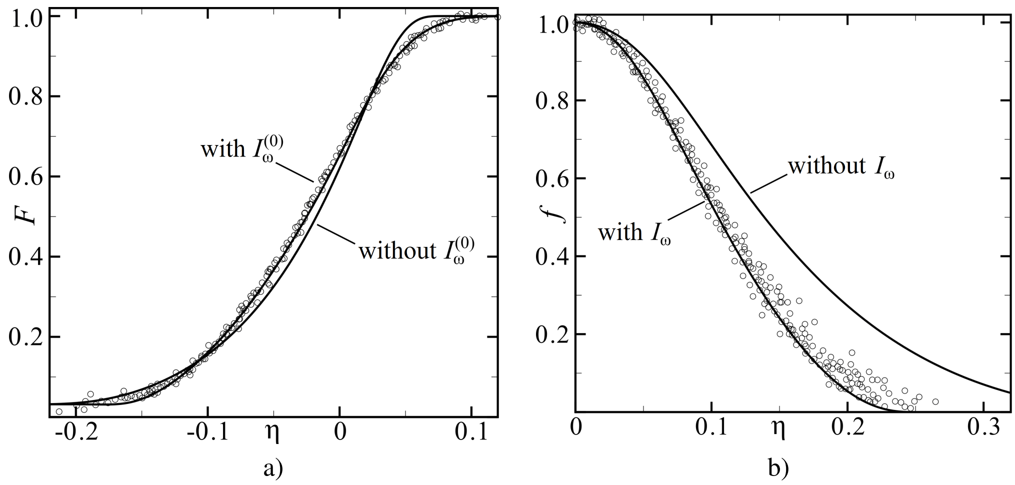

Figure 5: Velocity profile of: a) single-stream mixing layer, b) free plane jet far field, before and after the introduction of the extra source term in the SSG/LRR-ω turbulence model with modified coefficient values

It turns out that a turbulence model which correctly describes the temporal mixing layer, at the same time strongly distorts the single-stream mixing layer. Hence, this distortion is due to the effects absent in the temporal mixing layer: longitudinal gradients of velocity and turbulence variables and transverse velocity component connected to the gas ejection into the turbulent zone. To author's knowledge, the only attempt to explicitly take into account these effects in a turbulence model is paper Ref. 10 in which it is suggested to include an extra source term in the ε equation:

$$\frac{\partial \varepsilon}{\partial t} + \frac{\partial}{\partial x_k}\Big(\ldots\Big) = \frac{\varepsilon}{k}\left(\ldots + C_{\varepsilon 4}\frac{k^{5/2}}{\varepsilon}\nabla|\vec{V}| \cdot \nabla\gamma\right), \tag{12}$$

where γ is the intermittency factor.

It increases the production of ε at the low-velocity boundary of a mixing layer and decreases it at the high-velocity boundary which reduces the turbulent zone spread into $\eta < 0$ region and enhances — into $\eta > 0$ region.

In this paper, another source term is proposed which does not require the intermittency factor and is strictly Galilean invariant. In accordance with the observations made above, it depends on the longitudinal gradients of mean velocity and turbulence variables and on ejection velocity. Like the extra source term in Equation (12), it should behave as an "odd function" (i.e., to be of different signs in the regions $\eta < 0$ and $\eta > 0$). This source term is included in the ω equation.

To obtain the most general form of this term, let us restrict ourselves by using only mean velocity, k and ω gradients, but not individual R_{ij} components. If necessary, these retrictions would permit us to adapt the source term to the eddy viscosity models in the future. The second derivatives are not involved for simplicity. Velocity vector itself is not used as it is not Galilean invariant.

Using the above mentioned parameters, it is possible to form the following dimensionless aggregates:

$$N_{kk} = \frac{1}{k\omega^3}\frac{\partial \bar{u}_i}{\partial x_j}\frac{\partial k}{\partial x_i}\frac{\partial k}{\partial x_j}, \quad N_{k\omega} = \frac{1}{\omega^4}\frac{\partial \bar{u}_i}{\partial x_j}\frac{\partial k}{\partial x_i}\frac{\partial \omega}{\partial x_j},$$

$$N_{\omega k} = \frac{1}{\omega^4}\frac{\partial \bar{u}_i}{\partial x_j}\frac{\partial \omega}{\partial x_i}\frac{\partial k}{\partial x_j}, \quad N_{\omega\omega} = \frac{k}{\omega^5}\frac{\partial \bar{u}_i}{\partial x_j}\frac{\partial \omega}{\partial x_i}\frac{\partial \omega}{\partial x_j}.$$

Velocity gradient norms are not used in the denominators of these formulas since they can vanish in the uniform flow outside the turbulent zones.

In homogeneous turbulence and in the temporal mixing layer, all the expressions N_{kk}, $N_{k\omega}$, $N_{\omega k}$, $N_{\omega\omega}$ are identically zero. It can be shown that in self-similar spatial mixing layer $N_{kk} \equiv 0$ and $N_{k\omega} \equiv 0$, but $N_{\omega k} \neq 0$ and $N_{\omega\omega} \neq 0$. Moreover, both $N_{\omega k}$ and $N_{\omega\omega}$ behave as an "odd function" relative to the mixing layer center.

Two extra source terms have been successively added to the ω equation:

$$I_\omega^{(0)} = -C_{\omega 3} N_{\omega k} \omega^2, \quad J_\omega^{(0)} = -C'_{\omega 3} N_{\omega\omega} \omega^2.$$

Negative signs in these formulas allow to use positive $C_{\omega 3}$ and $C'_{\omega 3}$ values to get additional ω production at the low-velocity boundary of mixing layer and ω dissipation at the high-velocity boundary. It is found that $I_\omega^{(0)}$ is much more effective than $J_\omega^{(0)}$, and with $C_{\omega 3} \geq 20$ it produces the mixing layer velocity profile entirely matching the experimental data. $C_{\omega 3} = 21$ value is chosen which gives the potential core length estimation $L_{\mathrm{ini}} = 5.80$ and mixing layer width $D_{0.1} = 0.165$ without any extra turbulence model tuning. In Figure 5, a, velocity profiles are depicted without $I_\omega^{(0)}$ and with it.

A shortcoming of the $I_\omega^{(0)}$ source term is that with $C_{\omega 3} \geq 22$ the solution becomes unphysical: near the high-velocity mixing layer boundary, a running turbulent front appears on which instability develops. Moreover, even with $C_{\omega 3} = 21$ obtaining the stationary solution for the plane jet far field becomes a challenge.

Analysis has shown that the dimensionless aggregate $N_{\omega k}$ which enters the $I_\omega^{(0)}$ does not exceed 0.01 in the core of the mixing layer, but near its boundary $N_{\omega k}$ increases by several orders of magnitude. It is this uncontrollable growth of $N_{\omega k}$ which leads to the instability; consequently, $N_{\omega k}$ needs to be limited. The second reason for limiting is reduction of $I_\omega^{(0)}$ impact on the boundaries of turbulent zones, accurate description of which has been obtained earlier using the temporal mixing layer data.

Several modifications of $N_{\omega k}$ have been examined, which resulted in the following form of limiting:

$$I_\omega^{(1)} = -C_{\omega 3}\; 0.03 \tanh \frac{N_{\omega k}}{0.03}\; \omega^2.$$

With this limiting, the restriction $C_{\omega 3} \lesssim 21$ vanishes. To compensate for some loss of efficiency due to the limiting, $C_{\omega 3}$ has been increased to 22. With the presented modification, the width of the mixing layer practically leaves unchanged ($D_{0.1} = 0.164$) and L_{ini} equals 5.88. Velocity profile in the scale of Figure 5, a is undistinguishable from the earlier obtained profile with $I_\omega^{(0)}$. Now one can say that the goal of correct modeling of the spatial single stream mixing layer is reached.

The computation of the plane jet has showed that without $I_\omega^{(1)}$, jet half-width $\eta_{0.5}$ computed by the point where $f = 0.5$ equals to 0.139 whereas mean experimental value is 0.105. With $I_\omega^{(1)}$, it reduces to 0.098, i.e. $I_\omega^{(1)}$ increases the dissipation in the plane jet too much.

The following solution of this issue is proposed. It has been noticed that in self-similar mixing layer $N_{k\omega} \equiv 0$, but it is not zero in the plane jet. Let us use this additional term to independently calibrate the model against the plane jet data:

$$I_\omega^{(2)} = -C_{\omega 3}\; 0.03 \tanh \frac{N_{\omega k} - \beta N_{k\omega}}{0.03}\; \omega^2.$$

$N_{k\omega}$ is added with the negative sign to compensate the action of $N_{\omega k}$. A series of computations has been conducted with the use of $I_\omega^{(2)}$ with different β values. It is found that $\eta_{0.5} = 0.105$ is achieved when $\beta = 1.0$, so the final formulation of the extra source term is as follows:

$$I_\omega = -C_{\omega 3}\; 0.03 \tanh \frac{N_\omega}{0.03}\; \omega^2, \qquad C_{\omega 3} = 22, \qquad N_\omega = N_{\omega k} - N_{k\omega} = \frac{2\bar{\Omega}_{ij}}{\omega^4} \frac{\partial \omega}{\partial x_i} \frac{\partial k}{\partial x_j}, \qquad \bar{\Omega}_{ij} = \frac{1}{2}\left(\frac{\partial \bar{u}_i}{\partial x_j} - \frac{\partial \bar{u}_j}{\partial x_i}\right).$$

Plane jet velocity profiles obtained with and without I_ω depicted in Figure 5, b. With I_ω, the profile is slightly too sharp at the outer boundary, however it falls within the experimental data range.

5. Complete Reynolds equation system computations

SSG/LRR-ω turbulence model with the ability to enable the modifications proposed in the paper has been implemented within TsAGI in-house code designed to solve the complete unsteady Favre averaged Reynolds equation system. The numerical method used in conjunction with SSG/LRR-ω model is based on explicit second order finite volume Godunov-Kolgan-Rodionov scheme. Steady computations are conducted with local time stepping. Multiblock structured meshes are used.

A plane cold subsonic free jet has been computed. Nozzle width based Reynolds number $\mathrm{Re} = u_0 h/\nu$ is 6.7×10^6, Mach number is 0.30. Computational domain, the mesh and far field boundary conditions are shown in Figure 6. The region of fine mesh (of characteristic size $200h$) is surrounded by buffer blocks to move the computational domain boundaries $500h - 1000h$ far from the nozzle exit section which is positioned in the coordinate frame origin. The lower computational domain boundary is the jet symmetry plane.

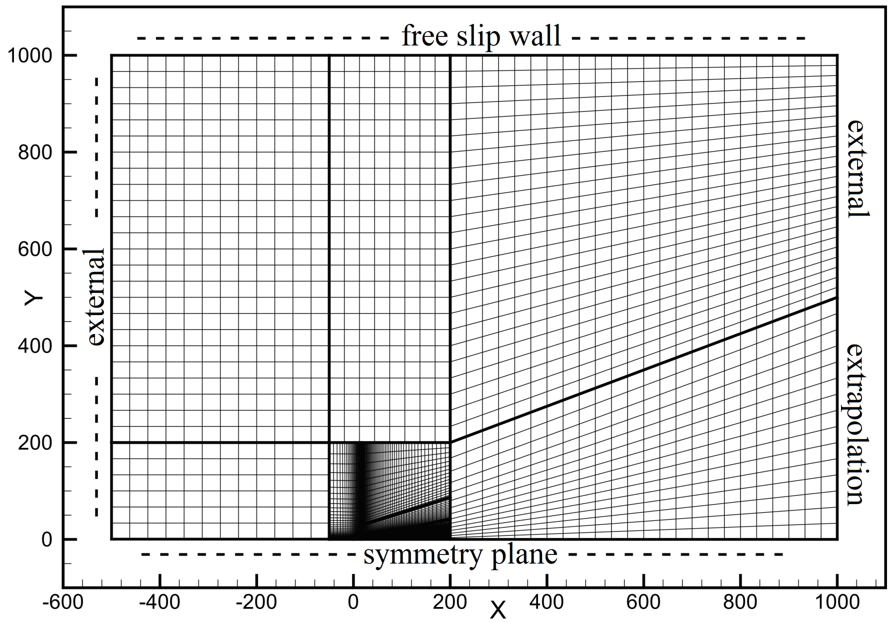

Figure 6: Computational domain, the mesh and far field boundary conditions in the computation of the plane jet

Turbulent boundary layer is modeled on the internal nozzle surface and contains 25 – 30 cells across it. To avoid the Kelvin–Helmholtz type instability, longitudinal mesh refinement near the nozzle lip is not made. The jet mixing layer contains 60 cells across it. In the jet far field, the mesh is refined in the transverse direction so that there are 70 cells across the jet half-width. Mesh convergence study has confirmed this mesh to be enough to accurately resolve the self-similar regions of the jet.

Longitudinal velocity flow field obtained with the modified SSG/LRR-ω model is shown in Figure 7.

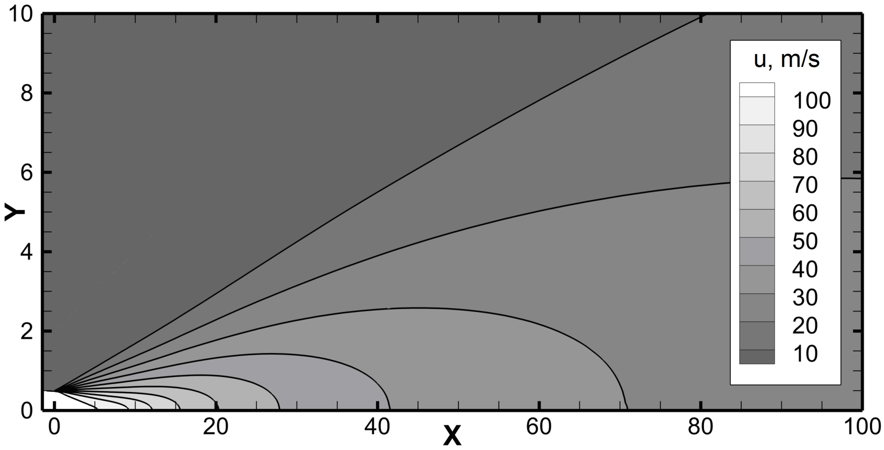

Figure 7: Longitudinal velocity flow field obtained with the modified SSG/LRR-ω model

The velocity profile of the jet mixing layer in $x/h = 3$ cross-section is compared to the self-similar profile obtained earlier in Figure 8, a. The far field velocity profiles ($x/h = 60$ and self-similar) are depicted in Figure 8, b. The differences between the profiles are insignificant, which confirms the applicability of self-similar approximation to the analysis conducted in the paper. The most pronounced discrepancies are on the low-velocity boundary of the turbulent zones and are due to the absence of the vertical wall above the nozzle exit section in the complete Reynolds equation system computations.

Axial velocity u_c distributions in the initial and part of the transitional region of the jet are shown in Figure 9, a. The modified model is compared to the original one. It is seen that the modified model does predict the potential core length $L_{\text{ini}} \approx 6$ whereas the experimental range is $5 \le L_{\text{ini}} \le 6$, which means the problem of potential core length overestimation is solved. The original model overpredicts L_{ini} nearly by a factor of 2.

In Figure 9, b, axial velocity distributions in the far field of the jet are presented. First, it can be observed that

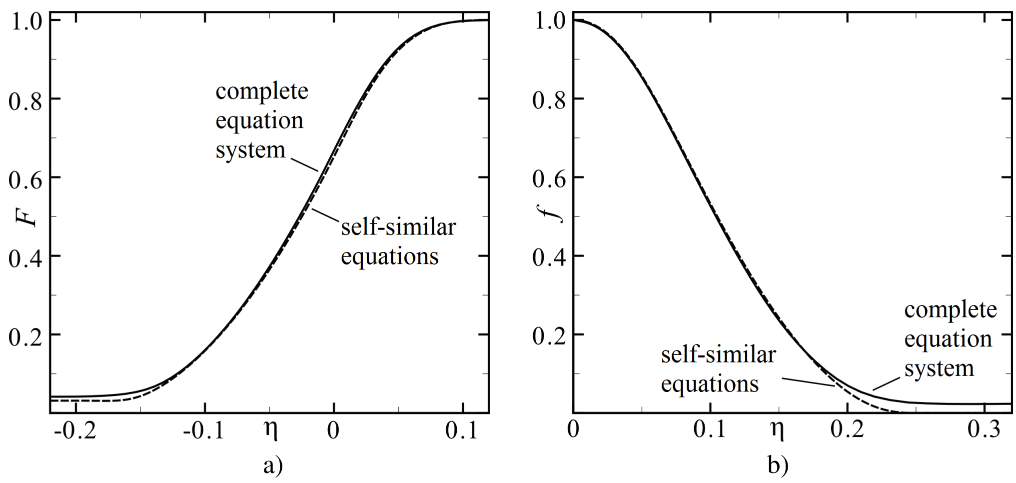

Figure 8: Velocity profiles comparison between the complete equation system and self-similar approximation: a) mixing layer b) jet far field

$(u_0/u_c)^2$ grows almost linearly obeying the self-similar relation, growth rate being in accordance with the experimental data. Second, the modified model corresponds to the experiments in $x/h > 15$ region while the original model shifts the velocity distribution downstream.

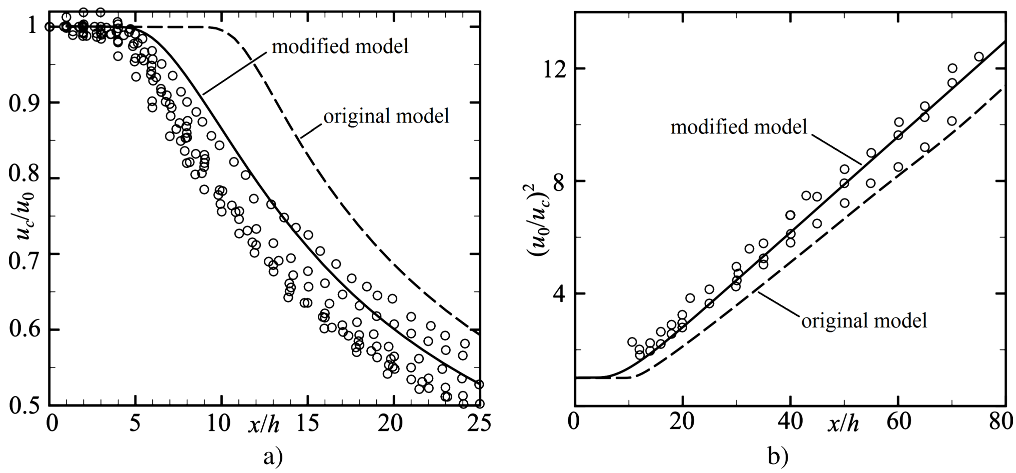

Figure 9: Axial velocity distribution: a) $x/h \leq 20$, b) $x/h \leq 80$

6. Conclusions

It is shown that turbulence diffusion models are not the main contributors to the discrepancies of the modern turbulence models in resolving the velocity profile of the single-stream mixing layers. Obtaining the correct solution is possible with the use of an extra source term in ω equation which accounts for the longitudinal gradients of velocity and turbulence variables and transverse velocity component connected to the gas ejection into the turbulent zone.

The proposed modifications to the SSG/LRR-ω turbulence model allow to obtain correct velocity profiles in the temporal and spatial mixing layers and in the free plane jet far field. It has been demonstrated in the computation of plane cold subsonic free jet that the modified model is superior to the original one in the whole flow field.

The reported study was partially supported by RFBR, research project No. 14-01-31546.

References

[1] Engblom W.A., Georgiadis N.J. and Khavaran A. Investigation of variable-diffusion turbulence model correction for round jets. In *11th AIAA/CEAS Aeroacoustics Conference*, AIAA Paper 2005-3085, May 2005.

[2] Vlasenko V., Bosniakov S., Mikhailov S., Morozov A. and Troshin A. Computational approach for investigation of thrust and acoustic performances of present-day nozzles. *Progress in Aerospace Sciences*, 46:141–197, 2010.

[3] Troshin A.I. A turbulence model with variable coefficients for calculating mixing layers and jets. *Fluid Dynamics*, 47:320–328, 2012.

[4] Cécora R.-D., Radespiel R., Eisfeld B. and Probst A. Differential Reynolds-stress modeling for aeronautics. *AIAA Journal*, 53:739–755, 2015.

[5] Speziale C.G., Sarkar S. and Gatski T.B. Modelling the pressure-strain correlation of turbulence: an invariant dynamical systems approach. *Journal of Fluid Mechanics*, 227:245–272, 1991.

[6] Wilcox D.C. Turbulence modeling for CFD. 2nd ed. DCW Industries. La Cañada, CA. 540 p., 1998.

[7] Pope S.B. Turbulent flows. Cambridge University Press. Cambridge. 802 p., 2000.

[8] El Baz A., Craft T.J., Ince N.Z. and Launder B.E. On the adequacy of the thin-shear-flow equations for computing turbulent jets in stagnant surroundings. *International Journal of Heat and Fluid Flow*, 14:164–169, 1993.

[9] Bell J.H. and Mehta R.D. Development of a two-stream mixing layer from tripped and untripped boundary layers. *AIAA Journal*, 28:2034–2042, 1990.

[10] Cho J.R. and Chung M.K. A $k - \epsilon - \gamma$ equation turbulence model. *Journal of Fluid Mechanics*, 237:301–322, 1992.